ELSEVIER

Polymer 43 (2002) 2445–2449

polymer

www.elsevier.com/locate/polymer

FT-IR spectroscopic study of hydrogen bonding in PA6/clay nanocomposites

Qiuju Wu, Xiaohui Liu, Lars A. Berglund*

Division of Polymer Engineering, Luleå University of Technology, S-97187 Luleå, Sweden

Received 10 October 2001; received in revised form 14 November 2001; accepted 7 December 2001

Abstract

Fourier transform infrared spectroscopy was used to investigate PA6/clay nanocomposites (PA6CN) with various cooling histories from the melt, including rapid cooling (water-quenched), middle-rate cooling (air-cooling) and slow cooling (mold-cooling). In contrast to pure PA6 dominated by the α-phase, the addition of clay silicate layers favor the formation of the γ-crystalline phase in PA6CN.

We focus on the reason why silicate layers favor the formation of γ-phase in PA6. Vaia et al. suggested that the addition of clay layers forces the amide groups of PA6 out of the plane formed by the chains. This results in conformational changes of the chains, which limits the formation of H-bonded sheets so that the γ-phase is favored. If this assumption is correct, PA6CN is expected to show some differences as compared with PA6 with respect to hydrogen bonding.

The silicate layers were indeed found to weaken the hydrogen bonding both in the α- and γ-phases. This was also confirmed by X-ray diffraction studies. The γ-phase is most likely concentrated in regions close to the silicate layers, whereas the α-phase is favored in the bulk matrix.

Keywords: PA6; Nanocomposite; Crystallization

1. Introduction

In recent years, organic–inorganic nanometer composites have attracted great interest from researchers since they frequently exhibit unexpected hybrid properties synergistically derived from two components. One of the most promising composite systems would be hybrids based on organic polymers and inorganic clay minerals consisting of layered structures, which belong to the general family of 2:1 layered silicates [1]. Compared to their micro- and macro-counterparts and the pristine polymer matrix, polymer/clay nanocomposites (PCN) exhibit improved tensile strength and moduli [2–7], decreased thermal expansion coefficient [4], decreased gas permeability [4–7], increased swelling resistance [8], enhanced ion conductivity [9–11], flammability [12,13] and so on. Presumably, the enhanced properties of PCN are due to the nanoscale structure, the large aspect ratio and surface area of the layered silicates and the corresponding strong interaction between polymer molecules and the silicate surface.

Dramatically improved mechanical properties of PA6/clay nanocomposites (PA6CN) were demonstrated by a group at the Toyota research center in Japan [14–16]. Since then, many PCN systems have been investigated and prepared. The majority of recent research work around PCN has focused on synthesis and characterization of physical properties. Although improved properties have been observed, the nature, origin and some unique phenomena in such nanocomposites are not well understood.

We prepared the PA6CN using a novel kind of co-intercalation organophilic montmorillonite clay prepared by melt compounding. A near 70% increase in modulus and strength was observed, the heat distortion temperature increased from 65 °C of PA6 up to 150 °C of PA6CN, and the notched Izod impact strength of PA6CN was doubled at 5 wt% clay. This is actually a higher impact strength than observed with the PA6CN reported in the present paper. The details of our property results will be published elsewhere.

In the present study, we attempt to improve our understanding of the interaction between silicate layers and PA6 at the molecular level. We apply Fourier transform infrared spectroscopy (FT-IR) and X-ray diffraction (XRD) and focus on hydrogen bonding and the different crystalline phases in PA6. We focus on the reason why silicate layers favor the formation of γ-phase in PA6. Vaia et al. suggested that the addition of clay layers forces the amide groups of PA6 out of the plane formed by the chains. This results in

* Corresponding author. Tel.: +46-920-4915-80; fax: +46-920-4910-84.
E-mail address: lars.berglund@mb.luth.se (L.A. Berglund).

0032-3861/02/$ - see front matter
PII: S0032-3861(01)00810-2

conformational changes of the chains, which limits the formation of H-bonded sheets and the γ-phase is favored [17]. If this assumption is correct, PA6CN is expected to show some differences as compared with PA6 with respect to hydrogen bonding.

2. Experimental

2.1. Materials

PA6, Ultramid B3 used in this study was manufactured by BASF. The cation exchange capacity of Na-montmorillonite was 80 mequiv./100 g. The water content was about 7 wt% in its original state (TGA method). The particle size was less than 20 μm. Epoxy resin ARALDITE GY 240, the diglycidyl ether of bisphenol A with a molecular weight of 360, was supplied by Ciba-Geigy.

In this article, the co-intercalation organophilic clay based on the classical ion-exchange organophilic clay was prepared as follows in two steps:

1. The ordinary organophilic clay was prepared via an ion exchange reaction in water using alkylammonium. Hundred grams of Na-montmorillonite was dispersed into 5000 ml of hot water using a homogenizer. Thirty grams of hexadecyl trimethyl ammonium bromide was then dissolved into hot water. It was poured into the Na-montmorillonite–water solution under vigorous stirring during 30 min to yield white precipitates. The precipitates were collected and washed with hot water three times, and then ground into the size of 20 μm after thorough drying in a vacuum oven. The obtained precipitate is a type of organophilic clay widely used in PCN.
2. Hundred and thirty grams of the ordinary organophilic clay obtained in step 1 and 20 g epoxy resin GY 240 were mixed in a Haake Recorder 40 mixer for 1 h. This resulted in what we term co-intercalation organophilic clay. The silicate interlayer distances were determined by XRD on specimens in powder form.

2.2. Preparation of PA6CN

A twin-screw extruder was used for the preparation of the nanocomposites. PA6 granules were dried in a vacuum oven at 120 °C for 24 h prior to blending with the organophilic clay. The temperature of the extruder was maintained at 220, 245, 245 and 230 °C from hopper to die, respectively. The screw speed was maintained at 180 rpm.

2.3. Characterization

FT-IR analyses were carried out using a Perkin Elmer 2000 spectrometer. Films of around 10 μm thickness (PA6 and PA6CN) were prepared as follows: the granule of PA6 or PA6CN was put between two glass slides; it was heated in an oil bath up to 250 °C. After complete melting of the granule, a load was applied to press the molten material into thin films. Three kinds of cooling conditions were then used. (1) Slow cooling: the films were cooled together with the mold in the oil bath from 250 to 20 °C by natural convection. (2) Middle rate cooling: the films were removed from the 250 °C oil bath and cooled in 20 °C air. (3) Rapid cooling: the films were removed from the 250 °C oil bath and quenched in a water bath at 20 °C.

PA6 specimens dominated by the α-phase were obtained from the slowly cooled material. Specimens dominated by the γ-phase were obtained by treating the α-phase specimens with iodine–potassium aqueous solution for 3 days. It was then treated with a sodium thiosulfate aqueous solution in order to remove the iodine. The crystallinity and crystalline phase structure was determined by XRD on a Siemens D5000 X-ray diffractometer. The Cu Kα radiation source was operated at 40 kV and 40 mA. Patterns were recorded by monitoring those diffractions that appeared from 2 to 30°. The scan speed was 2°/min.

3. Results and discussion

3.1. The effect of silicate layers on crystallization of PA6

The crystalline structure of PA6 under equilibrium conditions and at room temperature is the α-phase. It consists of all-*trans* chain conformations hydrogen-bonded into sheets (*ac*-plane); the intersheet stacking is controlled by van der Waals interactions [18–20]. Adjacent intrasheet chains are antiparallel, and the intrasheet hydrogen bonds shear in an alternating manner. For the γ-form of PA6, the chains are instead parallel and the hydrogen bonding is between chains in adjacent sheets. Typically the γ-form is an unstable form. It can be transformed into the α-form by annealing [19] or by treatment with a phenol aqueous solution [20,21].

The characteristic absorption peaks of the α-phase are 1478 cm^{-1} (CH_2 scissors vibration) [22], 1416 cm^{-1} (CH_2 scissors vibration) [22], 1373 cm^{-1} (amide III and CH_2 wag vibration) [22], 1199 cm^{-1} (CH_2 twist-wag vibration) [23], 959 cm^{-1} (CO–NH in plane vibration) [24] and 928 cm^{-1} (CO–NH in plane vibration) [24]. The characteristic peaks of the γ-phase were 1439 cm^{-1} (CH_2 scissors vibration) [25], 1369 cm^{-1} (CH_2 twist-wag vibration) [22], 1236 cm^{-1} (CH_2 twist-wag vibration) [26], 976 cm^{-1} (CO–NH in plane vibration) [27], 712 cm^{-1} (amide V) [27,28]. The characteristic peaks for the amorphous phase are still debated in the literature. The argument is focused on the assignment of peaks to mesomorphous or amorphous phases [25,29,30].

Fig. 1 shows the FT-IR spectra of PA6 films under various cooling conditions. The films quenched in 20 °C water, cooled in 20 °C air or cooled down in oil bath from 250 to 20 °C naturally were designated as PW, PA and PO, respectively. The spectrum of the slowly cooled PO specimens presented strong features of the α-phase associated

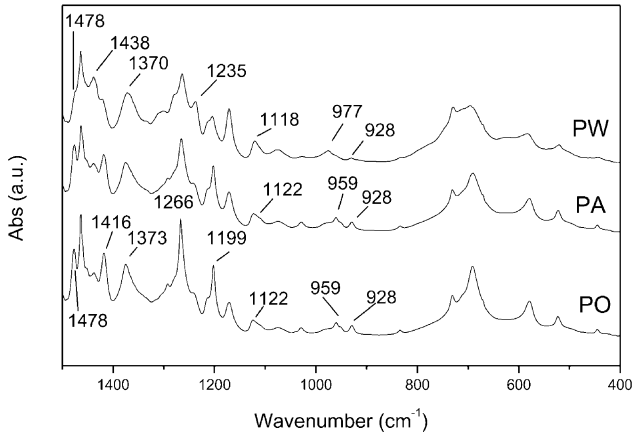

Fig. 1. FT-IR spectra of PA6 under various cooling conditions; PW: removed from the 250 °C oil bath and quenched in a water bath at 20 °C; PA: removed from the 250 °C oil bath and cooled in 20 °C air; PO: cooled down in oil bath from 250 to 20 °C by natural convection; the curves were stacked vertically for clarity.

with peaks at 1478, 1416, 1373, 1199, 959 and 928 cm^{-1}. No signal of the γ-phase was found in PO.

In contrast, water-quenched PW specimens showed peaks at 1438, 1370, 1235 and 977 cm^{-1} showing that the γ-phase was dominant. In addition, PW showed signs of the α-phase in the form of the shoulder at 1478 cm^{-1} and the weak peaks at 928 cm^{-1}. The spectrum of PA cooled at intermediate rate, showed that the α- and γ-phases coexisted. In summary, the α-phase dominates in PA6, while the γ-phase also can be observed if the specimen is quenched from the melt.

Fig. 2 shows the FT-IR spectra of PA6CN films under different cooling conditions. Similarly, the PA6CN films quenched in 20 °C water, cooled in 20 °C air or cooled down in oil bath from 250 to 20 °C are designated as N5W, N5A and N5O, respectively. In the spectra, 1040

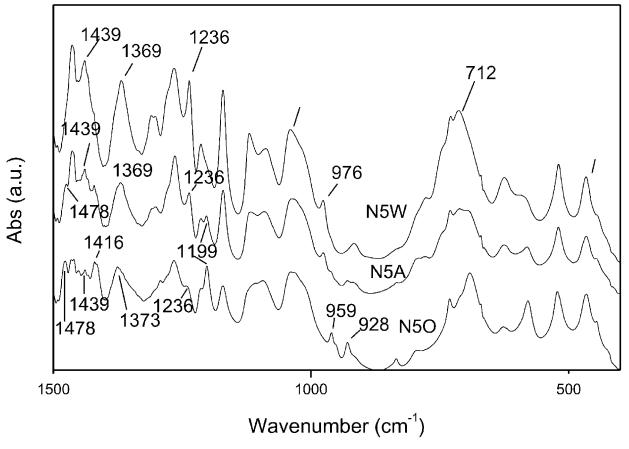

Fig. 2. FT-IR spectra of PA6/clay nanocomposite under various cooling conditions; N5W: removed from the 250 °C oil bath and quenched in a water bath at 20 °C; N5A: removed from the 250 °C oil bath and cooled in 20 °C air; N5O: cooled down in oil bath from 250 to 20 °C by natural convection; the curves were stacked vertically for clarity.

and 467 cm^{-1} is associated with the vibration modes of the clay [31,32]. In sharp contrast to PA6, all the PA6CN samples, regardless of cooling history, revealed the presence of γ-phase since peaks were observed at 1439 and 1236 cm^{-1}. No peaks associated with the α-phase were observed for N5W. In N5A, there were weak signals of the α-phase at 1478, 1199, 959 and 928 cm^{-1}. The intense α-peaks in N5O implied coexistence of two crystalline phases. In the spectrum of N5O, another characteristic peak of the α-phase at 1028 cm^{-1} did not show clearly, due to disturbance from the clay peak at 1040 cm^{-1}. The 1040 cm^{-1} peak in N5O was therefore broader than in N5W since the 1028 cm^{-1} peak became part of a shoulder of clay vibration at 1040 cm^{-1}.

In summary, the γ-phase becomes the dominant phase in the nanocomposite system. This phenomenon has been verified [15,16,33–36] by means of XRD or NMR. The behavior is consistent and independent of preparation methods, including in situ polymerization [15,16,35], melting intercalation with 12-aminolauric acid treated clay [6], octadecylammonium-treated [34] or silane treated clay [37]. The phenomenon is therefore explained by interaction between clay layers and PA6 molecules rather than by the effect of organic treatment.

In pure PA6, the γ-phase is metastable and consists of random hydrogen bonding between parallel chains [38]. Ito et al. observed that the mechanical properties of the α- and γ-phases, as well as the temperature dependence, are different for the two phases [39]. The α-phase exhibits a higher modulus below T_g but a more rapid decrease with temperature above T_g. This implies that the γ-phase has a higher heat distortion temperature. Thus, the relative fraction of the crystalline phases is expected to influence the mechanical properties of the nanocomposites. In addition, the more ductile γ-phase [40] may contribute greatly to the observed changes in mechanical properties of nanocomposites, especially the toughness.

The reason why the silicate layers favor the formation of γ-phase in PA6 still remains unclear. Vaia et al. suggested that the addition of clay layers forces the amide groups of PA6 out of the plane formed by the chains. This results in conformational changes of the chains, which limits the formation of H-bonded sheets and the γ-phase is favored [17]. If this assumption is correct, PA6CN is expected to show some differences as compared with PA6 with respect to hydrogen bonding.

3.2. The effect of silicate layers on hydrogen bonding

The NH stretching of polyamide spans a range of about 3100–3500 cm^{-1}. The major infrared bands of interest may be summarized as in Table 1. Fig. 3 shows the FT-IR spectra of α-phase PA6 with about 33% crystallinity (curve A), γ-phase PA6 with 31% crystallinity (curve B), γ-phase PA6CN with 49% crystallinity (curve C) and PA6CN with coexisting α- and γ-phases with 39% crystallinity (curve D).

Table 1
Band location and assignment

Band location (cm^{-1})	Assignment
3444	'Free' N–H stretch [41–43]
3300	Hydrogen-bonded N–H stretch in the crystalline phase [42]
3310	Hydrogen-bonded N–H stretch in the amorphous phase [41,42]
3070	Fermi-resonance of NH stretching with the overtone of amide II [27]
2930	Asymmetric CH_2 stretch [41,43]
2860	Symmetric CH_2 stretch [27]

The crystalline form and degree of crystallinity were determined by XRD. All curves in Fig. 3 have been normalized using the internal reference band at 1630 cm^{-1}. This was previously attributed to a carbonyl stretching vibration and shows no intensity change with different crystalline forms [44].

The intensity of the Fermi resonance of NH-stretching showed no big intensity difference among the four samples. However, a 13 cm^{-1} shift towards higher wavenumbers occurred in the γ-crystalline sample. Unexpected differences were observed on the absorption band corresponding to the hydrogen-bonded NH stretching vibration mode, between 3300 and 3310 cm^{-1}. In the γ-phase of PA6 (curve B), this peak was weaker than that in α-PA6 (curve A) due to distortion of the hydrogen-bonded sheet in the unit cell of the γ-phase [20]. In the nanocomposite, this peak (curve C) was further weakened as compared with pure PA6 (curve B), although both of them showed γ-phase, and PA6CN showed higher degree of crystallinity than pure PA6.

These observations show that the extent of hydrogen bonding in the γ-phase in PA6CN is reduced by the addition of silicate layers. The hydrogen-bonded sheets in the γ-phase are more disordered. We observed similar effects from the XRD pattern. In the γ-phase of PA6, the (020) reflection at $2\theta = 11.0°$ is assigned to the amide hydrogen-bonded layer (curve B, Fig. 4) [17,19]. This reflection is absent in PA6CN (curves C and D, Fig. 4). During crystallization, the silicate layers appear to greatly disturb the formation of hydrogen-bonded sheets in the γ-phase.

As indicated earlier, N5O showed coexisting α- and γ-phases. The FT-IR spectrum of this material (Fig. 3, curve D) is quite different from the individual α- and γ-phases in the high wavenumber zone. A broad and strong band was observed from 3450 to 3140 cm^{-1}. This range covers all the modes of vibration of 'free' NH, hydrogen-bonded NH in crystalline phase or hydrogen-bonded NH in amorphous phase. This is in contrast with the very sharp and strong peak at 3303 cm^{-1} for α-PA6 (Fig. 3, curve A). The corresponding peak in N5O was much weaker; meaning that the extent of hydrogen-bonded NH associated with the α-phase in N5O is much reduced. Since the N5O spectrum shows very clear α-peaks in the fingerprint zone (Fig. 2), we conclude that hydrogen-bonded NH is disturbed in the α-phase. The addition of silicate layers limit the formation of hydrogen-bonded sheets, and this favors formation of the γ-phase. Even in cases where the α-phase is present, the extent of hydrogen bonding is significantly reduced.

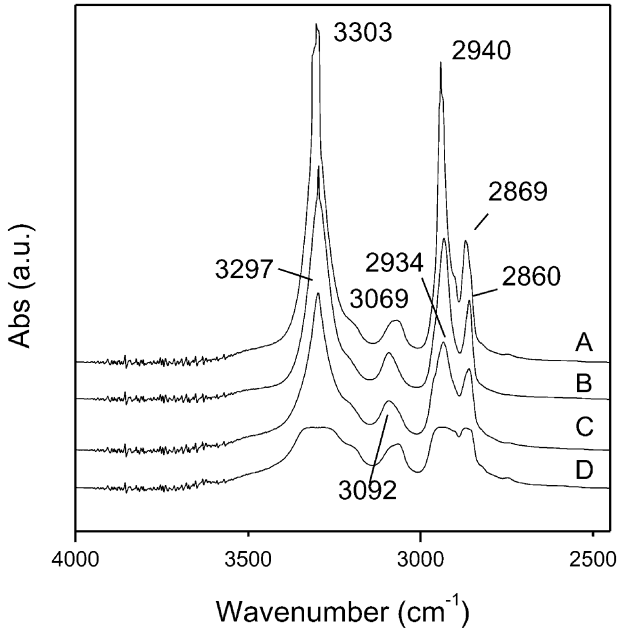

Fig. 3. FT-IR spectra of (A) α-phase PA6 with ~33% crystallinity; (B) γ-phase PA6 with ~31% crystallinity; (C) γ-phase PA6CN with ~49% crystallinity; (D) PA6CN with coexisting α- and γ-phases with ~39% crystallinity; the curves were stacked vertically for clarity.

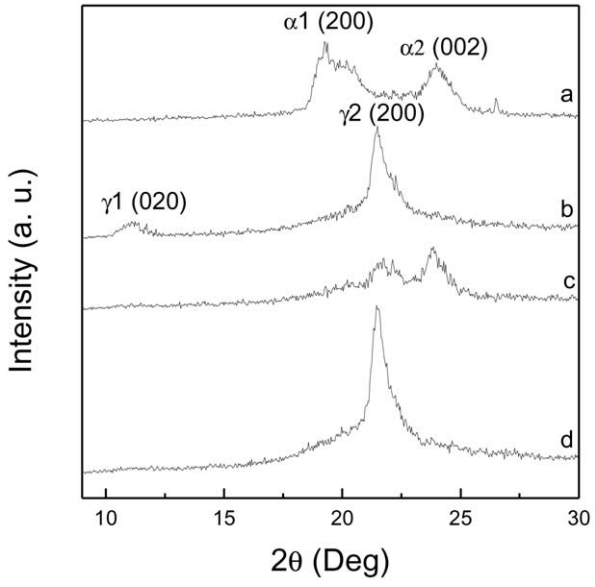

Fig. 4. XRD patterns of (a) α-phase PA6; (b) γ-phase PA6; (c) N5O (PA6CN is cooled down in oil bath from 250 to 20 °C by natural convection); (d) N5W (PA6CN is removed from the 250 °C oil bath and quenched in a water bath at 20 °C); the curves were vertically offset for clarity.

The effect is also apparent in the XRD data (Fig. 4). The α1 peak ($2\theta \approx 21°$) is sensitive to the distance between hydrogen-bonded chains inside the sheets. The α2 peak ($2\theta \approx 23°$) is sensitive to the separation distance between the sheets [45]. In PA6 (Fig. 4, curve A), both the α1 and α2 peaks are very distinct. The α1 peak is higher than the α2 peak. However, in N5O (Fig. 4, curve C), the α1 peak is barely visible, although the α-phase is clearly present according to data in the FT-IR finger print zone.

PA6 is most stable in the α-form. In γ-form, packing of the methylene units is optimum although the hydrogen bonding is poorer as compared with the α-form. The reason is that in the γ-phase, the hydrogen bonding distance is somewhat larger since it is primarily between sheets. As a consequence, the α-form is more stable than the γ-form by 0.34 kcal/mol per amide unit [20]. Our data show that the addition of silicate layers weakened the hydrogen bonding in PA6CN. While the degree of such weak-impact was different, most likely, depending on the distance between the fillers and the PA6 chains. In the weak-impact zone, for instance, the zone relatively far from the fillers, its crystalline structure still remained as α-like feature with poorer hydrogen bonding. However, in the strong-impact zone, located close to the silicate layers, the hydrogen bonding was disturbed too much and was too poor to form α-crystalline phase, thus showing the γ-crystalline feature.

4. Conclusions

The crystalline forms and the extent of hydrogen bonding were investigated in PA6CN. In contrast with neat PA6, addition of clay silicate layers favored the formation of γ-phase. This effect was stronger at higher cooling rates. The favoring of γ-phase at higher cooling rates is linked to unpublished observations showing molecular order in the nanocomposite also above the melting point.

Another effect apparent from our data is that the silicate layers weaken the hydrogen bonding both in the α- and γ-phases. Although the clay is likely to influence the thermodynamics of nucleation and growth processes during crystallization, we choose to focus on the hydrogen bonding effects. In a slightly different explanation from that of Vaia et al., one may speculate that the silicate primarily acts by limiting molecular mobility and the extent of hydrogen bonding. The favored conformations during crystallization then end up having the amide groups outside the plane and we obtain γ-phase. Since γ-phase is favored by the presence of silicate surfaces, we expect the γ-phase to dominate in regions close to the silicate, whereas the α-phase dominates further away.

References

[1] Pinnavaia TJ. Science 1983;220:365.
[2] Liu X, Wu Q, Berglund LA, Fan J, Qi Z. Polymer 2001;42:8235.
[3] Liu X, Wu Q. Polymer 2001;42:10013.
[4] Messersmith PB, Giannelis EP. Chem Mater 1994;6:1719.
[5] Messersmith PB, Giannelis EP. J Polym Sci: Polym Chem 1995;33:1047.
[6] Usuki A, Kojima Y, Kawasumi M, Okada A, Fukushima Y, Kurauchi T, Kamigaito O. J Mater Res 1993;8:1179.
[7] Yano K, Usuki A, Kurauchi T, Kamigaito O. J Polym Sci: Polym Chem 1993;31:2493.
[8] Burnside SD, Giannelis EP. Chem Mater 1994;6:2216.
[9] Vaia RA, Vasudevan S, Krawiec W, Scanlon LG, Giannelis EP. Adv Mater 1995;7:154.
[10] Aranda P, Ruiz-Hitzky E. Chem Mater 1992;4:1395.
[11] Wu J, Lerner MM. Chem Mater 1993;5:835.
[12] Gilman JW. J Appl Clay Sci 1999;15:31.
[13] Vaia RA, Price G, Ruth PN, Nguyen HT. J Appl Clay Sci 1999;15:67.
[14] Kojima Y, Usuki A, Kawasumi M, Okada A, Kurauchi T, Kamigaito O. J Polym Sci: Polym Chem 1993;31:983.
[15] Kojima Y, Usuki A, Kawasumi M, Okada A, Kurauchi T, Kamigaito O, Kaji K. J Polym Sci: Polym Phys 1994;32:625.
[16] Kojima Y, Usuki A, Kawasumi M, Okada A, Kurauchi T, Kamigaito O, Kaji K. J Polym Sci: Polym Phys 1995;33:1039.
[17] Lincoln DM, Vaia RA, Wang ZG, Hsiao BS. Polymer 2001;42:1621.
[18] Campoy I, Gomez MA, Macro C. Polymer 1999;40:4259.
[19] Ho J, Wei K. Macromolecules 2000;33:5181.
[20] Dasgupta S, Hammond W, Goddard WA. J Am Chem Soc 1996;118:12291.
[21] Kinoshita Y. Makromol Chem 1959;33:1.
[22] Schneider B, Schmidt P, Wichterle O. Coll Czech Commun 1962;27:1749.
[23] Doskocilova D, Pivcova H, Schnieder B, Cefelin P. Coll Czech Commun 1963;28:1867.
[24] Illers KH, Haberkorn H, Lanbo JB. J Macromol Sci, Phys 1972;B6:129.
[25] Rotter G, Ishida H. J Polym Sci, Part B: Polym Phys 1992;30:489.
[26] Tobin MC, Carrano MJ. J Chem Phys 1956;25:1044.
[27] Arimoto H. J Polym Sci: Part A 1964;2:2283.
[28] Miyake A. J Polym Sci 1960;44:223.
[29] Auriemma F, Petraccone V, Parravicini L, Corradini P. Macromolecules 1997;30:7554.
[30] Ziabicki A. Collect Czech Chem Commun 1957;22:64.
[31] Kloprogge JT, Frost RL. Vib Spectrosc 2000;23:119.
[32] Kloprogge JT, Frost RL. Appl Clay Sci 1999;15:431.
[33] Mathias L, Davis R, Jarrett W. Macromolecules 1999;32:7958.
[34] Liu L, Qi Z, Zhu X. J Appl Polym Sci 1999;71:1133.
[35] Kojima Y, Matsuoka T, Takahashi H, Kurauchi T. J Appl Polym Sci 1994;51:683.
[36] Wu Q, Liu X, Berglund LA. Macromol Rapid Commun 2001;22:1438.
[37] Akkapeddi MK. ANTEC'99, vol. XIV. New York City: Society of Plastics Engineers, Inc.; May 2–6 1999. p. 1619.
[38] Murthy NS. Polym Commun 1991;32:301.
[39] Ito M, Mizuochi K, Kanamoto T. Polymer 1998;39:4593.
[40] Joanny JF. Langmuir 1992;8:989.
[41] Skrovanek DJ, Howes SE, Painter PC, Coleman MM. Macromolecules 1985;18:1676.
[42] Deimede VA, Fragou KV, Koulouri EG, Kallitsis JK, Voyiatzis GA. Polymer 2000;41:9095.
[43] Schroeer LR, Cooper SL. J Appl Phys 1976;47:4310.
[44] Vasanthan N, Salem DR. J Polym Sci, Part B: Polym Phys 2001;39:536.
[45] Murthy NS, Curran SA, Aharoni SM, Minor H. Macromolecules 1991;24:3215.